Performance Analysis of Optical Reflecting Surface-Assisted Optical Space Shift Keying-based MIMO-FSO system

Narendra Vishwakarma, *Student Member, IEEE*, Swaminathan R., *Senior Member, IEEE*, Panagiotis D. Diamantoulakis, *Senior Member, IEEE,* and George K. Karagiannidis, *Fellow, IEEE*

***Abstract*—Recently, the use of reconfigurable intelligent surfaces (RIS) has gained popularity and is emerging as a promising technique to provide improved link reliability and enhanced coverage area. In this paper, we propose an optical reflecting surface (ORS)-assisted free space optics (FSO) communication system, which is based on optical space shift keying (OSSK) technique. Specifically, the closed-form expression for probability density function (PDF) of the ORS-assisted FSO channel is derived over Malaga turbulence model. Further, we have obtained the moment generating function (MGF) of the instantaneous signal-to-noise ratio (SNR) of the overall OSSK-based multiple-input multiple-output (MIMO)-FSO system. Using the derived channel statistics, an upper bound expression for the average bit error rate (BER) and a lower bound for the ergodic capacity are derived. Further, the asymptotic BER is utilized to calculate the diversity gain of the system. Numerical results are provided to corroborate the theoretical analysis of the system, along with insightful discussions. It is observed from the numerical results that the atmospheric turbulence and pointing errors have a negligible effect on the performance of the proposed system. Finally, a trade-off is noticed with respect to the average BER performance versus the spectral efficiency of the proposed system.**

***Index Terms*—Average bit error rate, ergodic capacity, Malaga distribution, multiple-input multiple-output (MIMO), optical reflecting surface (ORS), optical space shift keying (OSSK), pairwise error probability (PEP).**

I. Introduction

The 5^{th} generation (5G) wireless networks have now been deployed in most countries and will be expected to reach all over the world by 2023. Within this context, now the researchers are interested in the development of 6^{th} generation (6G) and beyond wireless technologies, which offer ultra-high bandwidth, extremely high data rates, low latency, and ultra-reliable links [1]. To meet these requirements, the reconfigurable intelligent surface (RIS) is recently proposed as a potential technique for the next-generation wireless communication systems [2]. The RIS module is a passive planar surface capable of modifying the properties of incoming electromagnetic waves such as amplitude, phase, and polarization [3]. For 6G wireless applications, the RIS-assisted radio frequency (RF) systems are being explored to boost reliability, signal-to-noise ratio (SNR), quality of service (QoS), and coverage area [4]. In [5], authors have proposed a RIS-assisted RF system in which data is transmitted in a dual-hop manner from transmitter to receiver via RIS. Further, the average symbol error probability (ASEP) performance of the RIS-assisted system was investigated over Rayleigh fading distribution based on the central limit theorem. In [6], the authors presented a more accurate performance analysis of the RIS-assisted RF system over Rician fading using the Laguerre series method for different modulation schemes. In [7], multiple RISs were deployed in a smart radio network to realize a cascaded RIS-assisted system and the performance was analyzed in terms of outage probability (OP), ASEP, and ergodic capacity (EC), over conventional binary modulation schemes by assuming Nakagami-m distribution. In [8], the authors have proposed a new RIS-phase modulation scheme by superimposing the message-bearing phase offsets on the typical RIS phase shifts to transmit the extra information and investigated the OP and ASEP of RIS-aided multiple-input single-output (MISO) system with the proposed phase modulation scheme.

Nevertheless, RF technology is currently experiencing major problems like low bandwidth and scarcity in its spectrum. In this regard, free space optics (FSO) communication, which offers licence-free spectrum, high data rates, and huge bandwidth, can be alternatively used in place of RF communication, especially in applications like wireless backhaul connectivity, metropolitan area networks, and remote connectivity [9]. Despite many advantages offered by FSO communication, the FSO links are generally affected by atmospheric turbulence, pointing errors, and adverse weather conditions such as snow, fog, haze, etc. [10]. In literature, many diversity schemes such as maximal ratio combining (MRC), selection combining (SC), and cooperative diversity schemes were proposed to mitigate the aforementioned drawbacks of the FSO communication [11]–[14]. Further, in [15], multiple-input multiple-output (MIMO) techniques were studied to enhance the performance of the FSO system under the effects of both turbulence and

This research is supported by the National Research Foundation, Singapore and Infocomm Media Development Authority under its Future Communications Research & Development Programme, Prime Minister's Research Fellows (PMRF) scheme, CRG scheme (File No. CRG/2021/0008813), MATRICS scheme (File No. MTR/2021/000553) of SERB, Govt. of India.

Narendra Vishwakarma and Swaminathan R are with the Department of Electrical Engineering, Indian Institute of Technology (IIT) Indore, (e-mails: phd1901102004@iiti.ac.in, swamiramabadran@iiti.ac.in)

Panagiotis D. Diamantoulakis and George K. Karagiannidis are with the Wireless Communications and Information Processing Group, Electrical and Computer Engineering Department, Aristotle University of Thessaloniki, 54124 Thessaloniki, Greece. George K. Karagiannidis is also with Cyber Security Systems and Applied AI Research Center, Lebanese American University (LAU), Lebanon. (e-mails: padiaman@auth.gr, geokarag@auth.gr)

pointing errors over the Gamma-Gamma fading distribution. In [16], [17], a backup RF link was introduced in parallel with the FSO link, termed as a hybrid FSO/RF system, for reliability improvement of the FSO system. In addition, the authors in [18] implemented the MIMO technique for the hybrid FSO/RF system over the generalized fading distributions. Furthermore, in [19], a dual-hop FSO system with an additional RF backup link to improve reliability of the relay-based FSO system was proposed and its performance was investigated.

In [20], a low complexity modulation scheme known as optical spatial modulation (OSM) was proposed for the MIMO-FSO system to achieve high spectral efficiency. Note that spatial modulation is an index modulation (IM) scheme in which the data information is transmitted in both antenna and signal spaces [21], [22]. Further, a special case of OSM is termed as optical spatial shift keying (OSSK), where only one transmitting aperture is active at a given time instant and the data is decoded as the index of the activated transmitting aperture [23]. In [24], the authors evaluated the performance of an FSO system based on the OSSK scheme over Gamma-Gamma distribution. However, in [24], the effect of pointing errors was neglected in the modeling of FSO channel. Moreover, in [25], the performance of a MISO-OSSK system was studied under jamming signals. The authors in [26] have analyzed the ergodic capacity of an OSSK-based FSO system by assuming Gamma-Gamma and negative-exponential distributions. Further, in [27], a mathematical framework was developed for the MIMO-OSSK-based FSO system in which average bit error rate (BER) and EC performances were investigated over non-generalized negative-exponential, lognormal, and Gamma-Gamma distributions.

Recently, the usage of RIS technology has also been extended to FSO scenario to combat the line-of-sight (LoS) link blockage issue due to buildings, trees, and other obstacles [28]. The RISs are made up of meta-surfaces that can be categorized as reconfigurable and non-reconfigurable surfaces depending on their configuration after fabrication [29]. The optical RIS-based FSO system has the advantage of lower hardware cost as compared to the FSO-based relaying system, since active components, which are essential at relay nodes, such as power amplifiers, encoders, decoders, etc., are not required in case of RIS [30]. In [31], the authors proposed a solution to the problem of skip-zones in FSO communication by using a RIS module between a source and a destination. Further, the cascaded FSO channel statistics were derived in [31] over the Gamma-Gamma distribution for investigating the performance of the system. In [32], the RIS-assisted FSO system was investigated over a large number of RIS elements to improve the performance and enhance the coverage area. Further, in [32], it was observed that the performance of the RIS-assisted FSO system improves drastically with an increase in the number of RIS elements. In [33], the authors presented a comprehensive performance of the RIS-assisted FSO system by investigating the metrics like OP, EC, and average bit error rate (ABER) over the generalized distributions. In [34], a RIS-aided mixed RF/FSO system is analyzed, where a single RF source is equipped with RIS and a single FSO link is used to connect relay and destination. Authors in [35] proposed the RIS-assisted hybrid FSO/RF system to improve the reliability in which both FSO and RF subsystems are assisted by RIS. Further, in [36], authors have considered the UAV-based RIS system with hybrid FSO/RF communication, where both FSO and RF links are equipped by a single RIS. In a nutshell, Table 1 provides a summary of the current research status of performance analysis of various RIS-based wireless system models.

A. Motivations and Contributions

In FSO communication, there are different obstacles in the line-of-sight (LOS) path, which are unsuitable for transmitting FSO signals and affect the FSO performance significantly [28]. In such situations, the use of ORS with the FSO communication can provide an alternate path for its data transmission [29], [31]. Further, the optical RIS, which is nearly passive in nature, has an advantage over the dual-hop relay-assisted systems in terms of lower hardware cost and power requirements [30]. Moreover, in the existing works on optical RIS [31]–[33], [35], [36], a single RIS or cascaded multiple RISs were considered for the FSO systems with a single transmitting and receiving apertures without any diversity combining techniques. Further, the OSSK-based FSO system is also prone to the shortcomings of the FSO system [23]–[27]. To overcome these limitations of the FSO-based systems, an optical reflecting surface (ORS)-assisted OSSK-based FSO system is proposed in our current work. Further, a system model considering an ORS-assisted OSSK-based FSO system with multiple apertures at the transmitter and the receiver has not been proposed and its performance has not been analyzed in the literature to the best of our knowledge. In addition, the cascaded FSO channel statistics as well as the absolute difference between two cascaded FSO channel statistics following Malaga distribution with pointing errors are also unexplored in the current literature. Therefore, we develop a mathematical framework, including the probability density function (PDF) and moment generating function (MGF) of the output instantaneous SNR to analyze the performance of the proposed system model.

Thus, the major contributions of our work are given as follows:

- The closed-form expressions are derived for the PDF of cascaded FSO channel with ORS and the PDF of absolute difference between two cascaded FSO channels. The FSO channel turbulence from source to ORS and from ORS to destination are modeled using the generalized Malaga distribution, including pointing errors.
- With the aid of the above-obtained expressions, the PDF and MGF of instantaneous SNR are derived for the proposed ORS-assisted OSSK-based MIMO-FSO system.
- Further, from the derived channel statistics, a tight upper bound on the average BER and a lower bound on the ergodic capacity are determined and useful insights from the derived analytical expressions are provided.
- The performance of the proposed ORS-assisted OSSK-based MIMO-FSO system is compared with the various existing conventional FSO systems such as single-

TABLE I: Literature summary on RIS-assisted RF and FSO system models

Ref.	System model	Number of RIS	Modulation technique	FSO/RF channel	Performance Metrics
[5]	RIS-aided RF system	Single	M-ary PSK	Rayleigh	ASEP
[6]	RIS-assisted RF system	Single	Binary modulation schemes	Rician	OP, ASEP, average channel capacity
[7]	Cascaded RIS-assisted RF system	Multiple	Binary modulation schemes	Nakagami-m	OP, EC, ASEP
[8]	MISO system with MRT scheme	Single	RIS-phase modulation scheme	Rayleigh	OP, ASEP
[31]	RIS-aided FSO system	Single	Binary modulation schemes	Gamma–Gamma	OP, ABER, EC
[32]	RIS-aided FSO system	Single	Binary modulation schemes	Gamma–Gamma	OP, ABER, EC
[33]	RIS-assisted FSO system	Single	Binary modulation schemes	Gamma–Gamma, Malaga, F-distribution	OP, ABER, EC
[34]	RIS-aided mixed FSO/RF with relay network	Two	Binary PSK	Gamma–Gamma/ Rayleigh	OP, ASEP
[35]	RIS-assisted hybrid FSO/RF system	Two	Binary PSK	Gamma–Gamma/ Rayleigh	OP, ABER, EC
[36]	UAV-based RIS-assisted hybrid FSO/RF system	Single	M-ary PSK	Gamma–Gamma/ Nakagami-m	ASER, channel capacity

link FSO system, OSSK-based MIMO-FSO system without ORS, and OSSK-based dual-hop (DH) decode-and-forward (DF) relaying system and detailed insights on the performance comparison are included in the numerical results.

- A high-SNR analysis is also considered to determine the asymptotic expressions for average BER and ergodic capacity, which are computationally less intensive.
- In addition, the diversity gain of the system is also determined from the asymptotic BER expressions. Furthermore, all the derived expressions are validated using Monte-Carlo simulations.

The remainder of this paper is structured as follows: Section II outlines the system and channel models for ORS-assisted FSO system with end-to-end channel PDF. In Section III, we investigate the average BER and ergodic capacity of the proposed system with the asymptotic analysis. In addition, a ratio test is also performed to test the convergence of the derived expressions. Section IV presents the numerical results with related inferences and technical insights. Finally, the paper is concluded in Section V.

II. System and Channel Models

A. System Model

We consider a $N_t \times N_r$ MIMO-FSO system assisted by an ORS based on the OSSK technique. Here, we assume that the ORS is adjusted such that the angle of incidence of the incoming optical signal is equal to the angle of reflection and the phase shift due to ORS is perfectly compensated using the phase-shift profile in [29]. In such a special case, the ORS is equivalent to a simple reflecting mirror, which redirects the incident optical signal to the receiver at the destination. The MIMO-FSO system comprises N_t number of LASER transmitters (i.e. source S) and N_r number of photo-detectors (i.e. destination D), which receives the FSO signals reflected by the ORS element as shown in Fig. 1. For simplicity and

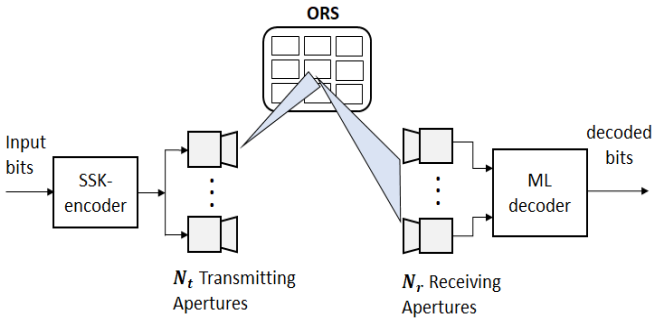

Fig. 1: The ORS-assisted OSSK-based MIMO-FSO system model

without the loss of generality, we assume that the perfect channel state information (CSI) is available at the receiver. At the OSSK encoder, the message bits are split into $\tau_b = \log_2 N_t$ bits. Depending upon the τ_b bits, one of the transmitting aperture is activated by the OSSK encoder and the rest of the optical transmitters will be in an idle state. Therefore, the OSSK-FSO system assists in achieving a spectral efficiency of $\tau_b = \log_2 N_t$. The received signal can be written as

$$\mathbf{Y} = \frac{\eta_f P_t}{N_r}\mathbf{H}\mathbf{X} + \mathbf{E}, \tag{1}$$

where $\mathbf{Y} \in \mathbb{R}^{N_r \times 1}$ denotes the received signal vector, η_f denotes the responsivity of the photo-detector, P_t is the FSO transmit power, $\mathbf{X} \in \{\mathbf{x}_i\}$, $1 \leq i \leq N_t$, $\mathbf{x}_i$ is the i^{th} column of an identity matrix $\mathbf{I}_{N_t}$, and $\mathbf{H} \in \mathbb{R}^{N_r \times N_t}$ represents the combined channel gain matrix. In $\mathbf{H}$ matrix, an element h_{ki} represents the combined channel coefficient between k^{th} receiver and i^{th} transmitter, and $\mathbf{E}$ is the additive white Gaussian noise (AWGN) vector having zero-mean and co-variance matrix $\sigma_n^2\mathbf{I}_{N_r}$, where σ_n^2 represents the noise variance.

In case of an OSSK-based scheme [23], the maximum likelihood (ML) detector is considered to decode the active transmitting aperture index at the receiver. Therefore, an estimate of the activated transmitting aperture index is given

by

$$\hat{i} = \arg\max_{i} f_{\mathbf{Y}}(\mathbf{Y}|\mathbf{x}_i, \mathbf{H}) = \arg\min_{i} \sum_{k=1}^{N_r} |Y_k - \eta_f P_t h_{ki}|^2, \quad (2)$$

where $\hat{i}$ is the estimated index of the transmitting aperture and $f_{\mathbf{Y}}(\mathbf{Y}|\mathbf{x}_i, \mathbf{H})$ is the PDF of output $\mathbf{Y}$ conditioned on $\mathbf{x}_i$ and $\mathbf{H}$. Further, the estimated aperture index $\hat{i}$ is decoded back into the corresponding τ_b bits.

B. Channel Model

The FSO channel from S to D is mainly affected by atmospheric turbulence, atmospheric attenuation, and pointing errors. The cascaded FSO channel gain h_{ki} by considering the effects of all the impairments is given by [28], [31]

$$h_{ki} = h_{a_1} h_{a_2} h_\ell h_p, \quad (3)$$

where h_{a_1} and h_{a_2} denote the atmospheric turbulence between S to ORS and ORS to D FSO links, respectively, h_p denotes the end-to-end pointing error impairments, and h_ℓ represents the atmospheric attenuation between S and D.

1) Pointing Errors Model: The pointing errors in the ORS-assisted FSO system are mainly due to beam jitter and ORS jitter, which are caused by mechanical vibrations at the transmitter and reflecting surface elements. The fading due to pointing errors in the ORS-assisted FSO system can be expressed as [28]

$$h_p \approx A_0 \exp(-2d^2/W_{z_{eq}}^2), \quad (4)$$

where $A_0 = [\text{erf}(v)]^2$, $W_{z_{eq}}^2 = \frac{W_z^2 \sqrt{\pi} \text{erf}(v)}{2v \exp(-v^2)}$, and $v = \frac{\sqrt{\pi} r_a}{\sqrt{2} W_z}$. Here, r_a denotes the aperture radius, $W_z = \phi_d L$ represents the beam width, ϕ_d denotes the beam divergence angle, and $L = L_1 + L_2$, where L_1 and L_2 are the distances between S to ORS and ORS to D, respectively. Further, in (4), $d = \tan(\theta_s) L_2 \approx \theta_s L_2$ is the instantaneous displacement between the center of the receiver and the actual receiving point of the beam, where θ_s denotes the superimposed pointing error angle, which is formed by the actual incident point at the receiver, reflection point at ORS, and the receiver center [28, Fig. 2]. In addition, θ_s is calculated as $\theta_s = \sqrt{\theta_{sx}^2 + \theta_{sy}^2}$, where $\theta_{sx} \approx \theta_x (1 + \frac{L_1}{L_2}) + 2\varphi_x$ is the horizontal component of θ_s and $\theta_{sy} \approx \theta_y (1 + \frac{L_1}{L_2}) + 2\varphi_y$ is the vertical component of θ_s. Moreover, θ_x and θ_y are the random variables (RVs) and they follow Gaussian distribution with zero-mean and variance σ_θ^2. Similarly, φ_x and φ_y are the deflection angles in horizontal and vertical planes, respectively, and are modeled as the Gaussian distribution with zero-mean and variance σ_φ^2. Therefore, the PDF of θ_s can be expressed as [32, eq. (3)]

$$f_{\theta_s}(\theta) = \frac{\theta}{\sigma_\theta^2 (1 + \frac{L_1}{L_2})^2 + 4\sigma_\varphi^2} e^{-\frac{\theta^2}{2\sigma_\theta^2 \left(1 + \frac{L_1}{L_2}\right)^2 + 8\sigma_\varphi^2}}. \quad (5)$$

Applying the RV transformation by using (4) and (5), we get the PDF of the pointing errors as

$$f_{h_p}(h) = \frac{\zeta}{A_0^\zeta} h^{\zeta - 1}, \quad 0 \le h \le A_0, \quad (6)$$

where $\zeta = \frac{W_{z_{eq}}^2}{4L^2 \sigma_\theta^2 + 16 L_2^2 \sigma_\varphi^2}$.

TABLE II: List of major parameters and notations

Parameter	Description
$\alpha_l > 0$	Large-scale atmospheric turbulence parameter [15, eq. (9)]
$\beta_l > 0$	Small-scale atmospheric turbulence parameter [15, eq. (9)]
Ω_l'	$\Omega_l' = \Omega_l + P_l \rho_l + 2\sqrt{P_l \rho_l \Omega_l} \cos\left(\phi_A^{(l)} - \phi_B^{(l)}\right)$
Ω_l	Average power of Line of sight (LoS) component
P_l	Total power of scattered components
$0 < \rho_l < 1$	Factor specifying the amount of scattered power coupled to the LoS component
y_l	$y_l = P_l(1 - \rho_l)$, average power of the off-axis scattered component
$\phi_A^{(l)}$	Deterministic phase of LoS component
$\phi_B^{(l)}$	Deterministic phase of coupled-to-LoS scattered component
$\text{erf}(\cdot)$	Error function [40, eq. (3.1.1)]
$K_a(\cdot)$	Modified Bessel function of second kind of order a
$G_{p\ q}^{m\ n}(\cdot)$	Meijer G-function [41, eq. (9.301)]

2) Atmospheric Turbulence Model: The Malaga distribution is assumed to model the atmospheric turbulence. It is a generalized fading distribution, which unifies most of the existing turbulence distribution models in the literature, and provides a great compliance with the published simulation data over all atmospheric turbulence regimes from weak to strong [37]. The unified PDF of h_{a_1} and h_{a_2} following the Malaga distribution is given by [38, eq. (24)]

$$f_{h_{a_l}}(h) = A_l \sum_{p=1}^{\beta_l} a_p^{(l)} h^{\frac{\alpha_l + p}{2} - 1} K_{\alpha_l - p}\left(2\sqrt{B_l h}\right), \quad (7)$$

where $l = \{1, 2\}$, $B_l = \frac{\alpha_l \beta_l}{y_l \beta_l + \Omega_l'}$, and A_l and $a_p^{(l)}$ are the constants, which are, respectively, given by

$$A_l = \frac{2\alpha_l^{\alpha_l/2}}{y_l^{1 + \alpha_l/2} \Gamma(\alpha_l)} \left(\frac{y_l \beta_l}{y_l \beta_l + \Omega_l'}\right)^{\beta_l + \alpha_l/2}, \quad (8)$$

$$a_p^{(l)} = \binom{\beta_l - 1}{p - 1} \frac{(y_l \beta_l + \Omega_l')^{1 - \frac{p}{2}}}{(p-1)!} \left(\frac{\Omega_l'}{y_l}\right)^{p-1} \left(\frac{\alpha_l}{\beta_l}\right)^{p/2}. \quad (9)$$

In (7), the modified Bessel function $K_a(\cdot)$ can be written in terms of Meijer G-function [39, eq. (07.34.03.0605.01)] and after some manipulations, we get the PDF of h_{a_l} as

$$f_{h_{a_l}}(h) = \frac{A_l h^{-1}}{2} \sum_{p=1}^{\beta_l} b_p^{(l)} G_{0\ 2}^{2\ 0}\left(B_l h \middle| \begin{matrix} - \\ \alpha_l, p \end{matrix}\right), \quad (10)$$

where $b_p^{(l)} = a_p^{(l)} B_l^{-(\alpha_l + p)/2}$. Note that other key notation and parameters are given in Table II. Additionally, the atmospheric attenuation is modeled using Beers-Lambert law as $h_\ell = \exp(-\alpha_w L)$, where α_w represents the weather dependent attenuation coefficient.

3) PDF of End-to-End FSO Channel: Firstly, we derive the PDF of the end-to-end turbulence of the FSO channel, which is the product of the turbulence of S to ORS and ORS to D links, i.e. $h_a^{eq} = h_{a_1} h_{a_2}$. Using the product of RVs, the PDF of h_a^{eq} can be written as

$$f_{h_a^{eq}}(x) = \int_0^\infty \frac{1}{t} f_{h_{a_1}}(t) f_{h_{a_2}}\left(\frac{x}{t}\right) dt. \quad (11)$$

By substituting $f_{h_{a_1}}(t)$ and $f_{h_{a_2}}(x)$ from (10) and using [39, eq. (07.34.21.0013.01)], $f_{h_a^{eq}}(x)$ is given by

$$f_{h_a^{eq}}(x) = \frac{A_1 A_2}{4x} \sum_{p=1}^{\beta_1} \sum_{q=1}^{\beta_2} b_p^{(1)} b_q^{(2)} G_{0\,4}^{4\,0}\left(B_1 B_2 x \middle| \begin{matrix} - \\ \mathcal{N}_1 \end{matrix} \right), \quad (12)$$

where $\mathcal{N}_1 = [\alpha_2, q, \alpha_1, p]$. Further, the end-to-end FSO channel coefficient is given by the product of turbulence and pointing errors, i.e. $h_{ki} = h_a^{eq} h_p h_\ell$. Similar to h_a^{eq}, the PDF of h_{ki} is expressed as

$$f_{h_{ki}}(x) = \int_{\frac{x}{h_\ell A_0}}^{\infty} \frac{1}{h_\ell t} f_{h_a^{eq}}(t) f_{h_p}\left(\frac{x}{h_\ell t}\right) dt \quad (13)$$

By substituting $f_{h_a^{eq}}(\cdot)$ and $f_{h_p}(\cdot)$ from (12) and (6), respectively, in (13) and after applying [39, eq. (07.34.21.0085.01)], $f_{h_{ki}}(x)$ is calculated as

$$f_{h_{ki}}(x) = \frac{A_1 A_2 B_1 B_2 \zeta}{4 A_0 h_\ell} \sum_{p=1}^{\beta_1} \sum_{q=1}^{\beta_2} b_p^{(1)} b_q^{(2)} G_{1\,5}^{5\,0}\left(\frac{B_1 B_2 x}{A_0 h_\ell} \middle| \begin{matrix} \zeta \\ \mathcal{N}_2 \end{matrix} \right), \quad (14)$$

where $\mathcal{N}_2 = [\zeta - 1, \alpha_2 - 1, q - 1, \alpha_1 - 1, p - 1]$.

III. Performance Analysis

In this section, the upper bound on average BER and lower bound on ergodic capacity of the ORS-assisted OSSK-based MIMO-FSO system are derived. The diversity gain of the system is obtained by applying the high-SNR approximations.

A. Average Bit Error Rate

A tight upper bound on BER of an OSSK system is given by [27, eq. (10)]

$$\text{BER} \leq \frac{1}{N_t \log_2 N_t} \sum_{i=1}^{N_t} \sum_{j=1}^{N_t} d_H(s_j, s_i) \text{PEP}^{j \to i}, \quad (15)$$

where $d_H(s_j, s_i)$ is the Hamming distance between symbols s_j and s_i, $\text{PEP}^{j \to i}$ denotes the pairwise error probability between s_j and s_i and it is expressed as

$$\text{PEP}^{j \to i} = \text{Q}\left(\frac{1}{N_r} \sqrt{\frac{\overline{\gamma}_{FSO} \log_2 N_t}{2} \sum_{k=1}^{N_r} |h_{ki} - h_{kj}|^2} \right), \quad (16)$$

where $\overline{\gamma}_{FSO} = \frac{\eta_f^2 P_t^2}{\sigma_n^2 \log_2 N_t}$ is the average SNR of the FSO link and $\text{Q}(\cdot)$ is the Gaussian Q-function. In addition, if $i = j$, then $d_H(s_j, s_i)$ is equal to zero, which represents the error-free decoding and its corresponding terms does not contribute to the BER. It is to be noted that the total number of mathematical operations required to calculate the upper bound on average BER for OSSK scheme is $N_t(3N_r - 1)$ [27]. In contrast, the computation complexities of the OSM-based system and Repetition Coding (RC)-based pulse amplitude modulation (PAM) system are given by $\mathcal{M} N_t (3N_r - 1)$ and $\mathcal{M}(2N_t N_r + N_r - 1)$, respectively, where $\mathcal{M}$ is the modulation order [22]. Therefore, the OSSK-based FSO MIMO system is computationally less expensive than the above-mentioned OSM and RC-PAM systems.

Theorem 1: The PDF of magnitude of difference between two independent cascaded FSO channels (i.e. $U_{kij} = |h_{ki} - h_{kj}|$), with PDF of each channel following (14), is given by

$$f_{U_{kij}}(u) = \frac{(A_1 A_2 \zeta)^2 B_1 B_2}{8 A_0 h_\ell} \sum_{p=1}^{\beta_1} \sum_{q=1}^{\beta_2} \sum_{r=1}^{\beta_1} \sum_{s=1}^{\beta_2} b_p^{(1)} b_q^{(2)} b_r^{(1)} b_s^{(2)} \times \sum_{n=0}^{\infty} \left(\frac{-B_1 B_2}{A_0 h_\ell} \right)^n \frac{u^n}{n!} G_{7\,7}^{5\,6}\left(1 \middle| \begin{matrix} \mathcal{N}_3 \\ \mathcal{N}_4 \end{matrix} \right), \quad (17)$$

Proof: See Appendix A. ∎

Theorem 2: The PDF of instantaneous SNR of the ORS-assisted OSSK-based MIMO-FSO system is given by

$$f_{\gamma_{ij}}(\gamma) = \sum_{n=0}^{\infty} D_n \frac{\gamma^{\frac{n+N_r-2}{2}}}{\Gamma\left(\frac{N_r+n}{2}\right)} \quad (18)$$

Proof: See Appendix B. ∎

It is important to note that the obtained PDF of the instantaneous SNR has a single power series with a power exponent of γ. Now, it is easier to evaluate the integrals based on this power series to calculate the average BER and ergodic capacity expressions for ORS-assisted OSSK-based MIMO FSO system.

Therefore, the average PEP of the MIMO-OSSK is determined by averaging PEP over instantaneous SNR γ_{ij} as

$$\text{APEP}^{j \to i} = \int_0^{\infty} \text{Q}\left(\frac{1}{N_r} \sqrt{\frac{\log_2 N_t}{2} \gamma} \right) f_{\gamma_{ij}}(\gamma) d\gamma. \quad (19)$$

Using the relationship $\text{Q}(x) = \frac{1}{2}\text{erfc}\left(\frac{x}{\sqrt{2}}\right)$ and after utilizing [40, eq. 4.1.18], the average PEP is given by

$$\text{APEP}^{j \to i} = \sum_{n=0}^{\infty} \frac{D_n \Gamma\left(\frac{n+N_r+1}{2}\right)}{\sqrt{\pi}(n+N_r)\Gamma\left(\frac{n+N_r}{2}\right)} \left(\frac{2N_r}{\sqrt{\log_2 N_t}} \right)^{N_r+n} \quad (20)$$

The upper bound on the average BER of the OSSK-based MIMO-FSO system can be written as

$$\text{ABER} \leq \frac{1}{N_t \log_2 N_t} \sum_{i=1}^{N_t} \sum_{j=1}^{N_t} d_H(s_j, s_i) \times \text{APEP}^{j \to i} \quad (21)$$

Since the channel RVs h_{ki} and h_{kj} are independent and identically distributed (i.i.d.), the double summation term $\sum_{i=1}^{N_t} \sum_{j=1}^{N_t} d_H(s_j, s_i)$ in (21) can be simplified as $\frac{N_t^2 \log_2 N_t}{2}$ [23, eq. (11)]. Finally, by substituting (20) in (21), the upper bound expression for the average BER of ORS-assisted MIMO-FSO system is given by

$$\text{ABER} \leq \frac{N_t}{2\sqrt{\pi}} \sum_{n=0}^{\infty} \frac{D_n \Gamma\left(\frac{n+N_r+1}{2}\right)}{(n+N_r)\Gamma\left(\frac{n+N_r}{2}\right)} \left(\frac{2N_r}{\sqrt{\log_2 N_t}} \right)^{N_r+n} \quad (22)$$

It can be observed from (22) that the derived upper bound will increase by increasing the transmitting apertures N_t, keeping other parameters constant. Consequently, the average BER performance will degrade. However, the spectral efficiency of the OSSK-based FSO system, which is given by $\tau_b = \log_2 N_t$

bits/s/Hz, will improve by increasing N_t. Therefore, a trade-off exists between the average BER and spectral efficiency of the proposed ORS-assisted OSSK-based MIMO FSO system. Further, the upper bound expression in (22) is obtained as an infinite summation containing a converging power series, which can be verified by performing a convergence test (i.e. Cauchy ratio test).

Remark 1: The average BER of an ORS-assisted MIMO-FSO system for a special case when $N_t = 2$ and $N_r = 1$ can be reduced as

$$\text{ABER} \leq \frac{1}{\sqrt{\pi}} \sum_{n=0}^{\infty} \frac{D_n \Gamma\left(\frac{n+2}{2}\right)}{\Gamma\left(\frac{n+3}{2}\right)} 2^n \tag{23}$$

B. Ergodic Capacity Analysis

For an OSSK-based MIMO-FSO system, a more practical capacity can be defined in terms of discrete-input continuous-output memoryless channel (DCMC) capacity as [23]

$$C_D \approx 2\log_2 N_t - \log_2 \Bigg(N_t + \sum_{i=1}^{N_t} \sum_{\substack{j=1 \\ j\neq i}}^{N_t} \exp\Big(-\frac{\overline{\gamma}_{FSO}}{2N_r^2} \times \log_2 N_t \sum_{k=1}^{N_r} (h_{ki} - h_{kj})^2 \Big) \Bigg). \tag{24}$$

Further, by utilizing the Jensen's inequality [27, eq. (21)], a lower bound expression for the DCMC capacity can be determined as

$$C_D^{avg} \geq 2\log_2 N_t - \log_2 \Bigg(N_t + \sum_{i=1}^{N_t} \sum_{\substack{j=1 \\ j\neq i}}^{N_t} \mathbb{E}\Big[\exp\Big(-\frac{\overline{\gamma}_{FSO}}{2N_r^2} \times \log_2 N_t \sum_{k=1}^{N_r} (h_{ki} - h_{kj})^2 \Big) \Big] \Bigg) \tag{25}$$

where $\mathbb{E}[\cdot]$ represents the expectation operator. The maximum achievable capacity can be obtained as $\overline{\gamma}_{FSO} \to \infty$ in (25). Since $\exp(\cdot)$ function in (25) will be equal to zero as $\overline{\gamma}_{FSO} \to \infty$, the maximum achievable capacity is given by

$$C_{D(max)}^{avg} = \log_2 N_t. \tag{26}$$

The expectation term on the right hand side of (25) can be simplified as

$$\mathbb{E}\left[\exp\left(-\frac{\log_2 N_t}{2N_r^2} \sum_{k=1}^{N_r} \gamma_{kij} \right) \right] = \prod_{k=1}^{N_r} \mathbb{E}\left[\exp\left(-\frac{\gamma_{kij} \log_2 N_t}{2N_r^2} \right) \right] \tag{27}$$

where γ_{kij} is given in Appendix B. Furthermore, the above expression can be given in terms of moment generating function (MGF) as

$$\prod_{k=1}^{N_r} \mathbb{E}\left[\exp\left(-\frac{\gamma_{kij} \log_2 N_t}{2N_r^2} \right) \right] = \prod_{k=1}^{N_r} \Psi_{\gamma_{kij}}\left(-\frac{\log_2 N_t}{2N_r^2} \right) = \Psi_{\gamma_{ij}}\left(-\frac{\log_2 N_t}{2N_r^2} \right) \tag{28}$$

where the MGF functions $\Psi_{\gamma_{kij}}(\cdot)$ and $\Psi_{\gamma_{ij}}(\cdot)$ are given by (44) and (46), respectively. Further, using (28), the lower bound on the capacity in (25) can be rewritten as

$$C_D^{avg} \geq 2\log_2 N_t - \log_2 \left(N_t + \sum_{i=1}^{N_t} \sum_{\substack{j=1 \\ j\neq i}}^{N_t} \Psi_{\gamma_{ij}}\left(-\frac{\log_2 N_t}{2N_r^2} \right) \right) \tag{29}$$

Proposition 1: The expression for lower bound on the ergodic capacity of an OSSK-based MIMO-FSO system is given as

$$C_D^{avg} \geq 2\log_2 N_t - \log_2 \left(N_t + (N_t^2 - N_t) \times \sum_{n=0}^{\infty} D_n \left(\frac{2N_r^2}{\log_2 N_t} \right)^{\frac{n+N_r}{2}} \right) \tag{30}$$

Proof: By putting $t = \frac{\log_2 N_t}{2N_r^2}$ in (46) and substituting its value in (29), we get the final expression for C_D^{avg} as (30). ■

Further, in (30), if $\overline{\gamma}_{FSO} \to \infty$, then the maximum value of ergodic capacity is obtained as $C_D^{avg} = \log_2 N_t$, which validates the correctness of the derived ergodic capacity expression. [1]

Remark 2: For a special case, when $N_t = 2$ amd $N_r = 1$, the bound on the ergodic capacity can be simplified as

$$C_D^{avg} \geq 1 - \log_2 \left(1 + \sum_{n=0}^{\infty} D_n 2^{\frac{n+N_r}{2}} \right) \tag{31}$$

C. High Average SNR Analysis and Diversity Gain

Here, we derive a less complicated expression for the upper bound on average BER using high-SNR approximations. In (22), by assuming $\overline{\gamma}_{FSO} \to \infty$, the dominant term will be obtained by taking $n = 0$ and the asymptotic average BER expression is simplified as

$$\text{ABER}^{\infty} \leq \left(\frac{1}{\overline{\gamma}_{FSO}} \right)^{\frac{N_r}{2}} \frac{N_t \Gamma\left(\frac{N_r+1}{2}\right)}{2\sqrt{\pi} N_r \Gamma\left(\frac{N_r}{2}\right)} \left[\frac{N_r (A_1 A_2 \zeta)^2 B_1 B_2}{8 A_0 h_\ell \sqrt{\log_2 N_t}} \times \sqrt{\pi} \sum_{p=1}^{\beta_1} \sum_{q=1}^{\beta_2} \sum_{r=1}^{\beta_1} \sum_{s=1}^{\beta_2} b_p^{(1)} b_q^{(2)} b_r^{(1)} b_s^{(2)} G_{7\,7}^{5\,6} \left(1 \middle| \begin{matrix} \mathcal{N}_5 \\ \mathcal{N}_6 \end{matrix} \right) \right]^{N_r}, \tag{32}$$

where $\mathcal{N}_5 = [0, 1-\zeta, 1-\alpha_2, 1-q, 1-\alpha_1, 1-p, \zeta]$ and $\mathcal{N}_6 = [\zeta - 1, \alpha_2 - 1, s-1, \alpha_1 - 1, r-1, -\zeta, 0]$. From the above expression, it can be seen that $\text{ABER}^{\infty} \propto (1/\overline{\gamma}_{FSO})^{\frac{N_r}{2}}$ and the diversity gain is given by $N_r/2$. It is observed that the diversity gain is independent of the factors like turbulence and pointing error parameters unlike the general M-ary modulation-scheme-based FSO system without OSSK scheme [15], [31]. This is because, the pair-wise error probability (PEP), which is used for calculating the average BER of OSSK system, depends on the difference between the channel gains and does not depend on the individual FSO channel gain. In addition, the fluctuations in the atmospheric turbulence or

[1] It is to be noted that $\overline{\gamma}_{FSO}$ is inside the term D_n, which is given in Appendix B.

pointing errors do not greatly contribute to the difference in the channel gains. Hence, the diversity gain of the OSSK system is independent of the turbulence and pointing error parameters.

Similarly, the less-complicated asymptotic expression for the given capacity bound can be determined by assuming high value of $\overline{\gamma}_{FSO}$ in (30) and the final expression is given as

$$C_D^{\infty} \geq 2\log_2 N_t - \log_2 \left[N_t + (N_t^2 - N_t) \left(\frac{2N_r^2 C_0^2}{\log_2 N_t} \right)^{\frac{N_r}{2}} \right], \tag{33}$$

where

$$C_0 = \frac{\Gamma\left(\frac{1}{2}\right)}{\left(\overline{\gamma}_{FSO}\right)^{\frac{1}{2}}} \left[\frac{(A_1 A_2 \zeta)^2 B_1 B_2}{16 A_0 h_\ell} \times \sum_{p=1}^{\beta_1} \sum_{q=1}^{\beta_2} \sum_{r=1}^{\beta_1} \sum_{s=1}^{\beta_2} b_p^{(1)} b_q^{(2)} b_r^{(1)} b_s^{(2)} G_{7\,7}^{5\,6} \left(1 \middle| \begin{matrix} \mathcal{N}_7 \\ \mathcal{N}_8 \end{matrix} \right) \right]. \tag{34}$$

It can be seen from (33) and (34) that by increasing the value of N_r, the factor $C_0^{N_R}$ will decrease significantly with increase in $\overline{\gamma}_{FSO}$. Consequently, there will be an improvement in the ergodic capacity value and the average SNR required to achieve the maximum capacity will be reduced. However, the maximum capacity value will be always equal to $\log_2 N_t$ as given by (26), which is independent of N_r.

D. Convergence Test

To test the convergence of the average BER and capacity expressions in (22) and (30), respectively, a Cauchy ratio test is performed on the power series of MGF of $\gamma_{kij}(-t)$ in (44), which is used to calculate the average BER and ergodic capacity bounds. Further, if the infinite series in $\gamma_{kij}(-t)$ is convergent, then the $\Psi_{\gamma_{ij}}(-t)$ is also convergent and consequently, we can say that the derived average BER and ergodic capacity expressions will be absolutely convergent. For a given series $\sum_{n=0}^{\infty} u_n$, if the following condition is satisfied, i.e.

$$\lim_{n\to\infty} \left| \frac{u_{n+1}}{u_n} \right| < 1, \tag{35}$$

then the given series is said to be absolutely convergent. From (44), let us assume the series coefficient $u_n = C_n t^{-\frac{n+1}{2}}$ and the ratio of series coefficient is defined as

$$\left| \frac{u_{n+1}}{u_n} \right| = \left| \frac{\left(\frac{-B_1 B_2}{A_0 h_\ell} \right)^{n+1} \frac{t^{-\frac{n+2}{2}} \Gamma\left(\frac{n+2}{2}\right)}{(n+1)! \overline{\gamma}_{FSO}^{\frac{n+2}{2}}} G_{7\,7}^{5\,6} \left(1 \middle| \begin{matrix} \mathcal{N}_7 \\ \mathcal{N}_8 \end{matrix} \right)}{\left(\frac{-B_1 B_2}{A_0 h_\ell} \right)^{n} \frac{t^{-\frac{n+1}{2}} \Gamma\left(\frac{n+1}{2}\right)}{n! \overline{\gamma}_{FSO}^{\frac{n+1}{2}}} G_{7\,7}^{5\,6} \left(1 \middle| \begin{matrix} \mathcal{N}_3 \\ \mathcal{N}_4 \end{matrix} \right)} \right| \tag{36}$$

where $\mathcal{N}_7 = 0, n-\zeta+2, n-\alpha_2+2, n-q+2, n-\alpha_1+2, n-p+2, \zeta$ and $\mathcal{N}_8 = \zeta-1, \alpha_2-1, s-1, \alpha_1-1, r-1, n-\zeta+1, n+1$. After simplification, we get

$$\left| \frac{u_{n+1}}{u_n} \right| = \left[\frac{\Gamma\left(\frac{n+2}{2}\right)}{(n+1)\Gamma\left(\frac{n+1}{2}\right)} \right] F \tag{37}$$

where $F = \left| \frac{-B_1 B_2 G_{7\,7}^{5\,6} \left(1 \middle| \begin{matrix} \mathcal{N}_7 \\ \mathcal{N}_8 \end{matrix} \right)}{A_0 h_\ell (t\overline{\gamma}_{FSO})^{1/2} G_{7\,7}^{5\,6} \left(1 \middle| \begin{matrix} \mathcal{N}_3 \\ \mathcal{N}_4 \end{matrix} \right)} \right|$. Here, the constant F will always give a positive real number for all n and t.

TABLE III: Truncation accuracy of summation limits for BER

$\overline{\gamma}_{FSO}$	Final values of BER for truncation limit n				Upper limit
	5	8	11	12	
15	0.200909	0.759853	0.755896	0.755896	$n=11$
20	0.628429	0.633963	0.633950	0.633950	$n=11$
25	0.699009	0.699009	0.699009	0.699009	$n=11$
30	0.298805	0.298805	0.298805	0.298805	$n=11$

TABLE IV: Truncation accuracy of summation limits for capacity

$\overline{\gamma}_{FSO}$	Final values of capacity for truncation limit n				Upper limit
	3	5	11	12	
25	1.689138	1.689459	0.350584	0.350584	$n=11$
30	1.816396	1.816400	1.785124	1.785124	$n=11$
40	1.935630	1.935631	1.935627	1.935627	$n=11$

From (37), it can be clearly observed that the powers of n in denominator is one higher than numerator and after applying the limit $n \to \infty$, the expression will tend to zero. Therefore, the obtained average BER and ergodic capacity expressions are absolutely convergent.

IV. Numerical and Simulation Results

This section presents the analytical and simulation results of the proposed system model for average BER and ergodic capacity. The theoretical results are verified by performing the Monte-Carlo simulations for 10^6 data bits. In the proposed ORS-assisted FSO system, we have assumed the link distances as $L_1 = L_2 = 250$ m. In addition, the other system parameters are assumed as follows: FSO wavelength $\lambda_F = 1550$ nm, $\sigma_\theta = 1$ mrad, $\sigma_\varphi = 0.5$ mrad, $r_a = 0.1$ m, $\phi_d = 8$ mrad, $\rho_l = 0.999$, $\phi_A^{(l)} - \phi_B^{(l)} = \pi/2$, $\Omega_l = 1.3265$, and $P_l = 0.2158$, unless and otherwise stated [27], [32]. It is to be noted that the values of turbulence and other parameters for S to ORS and ORS to D links are assumed as $\alpha_1 = \alpha_2 = \alpha$ and $\beta_1 = \beta_2 = \beta$.

The upper limits used for truncating the infinite series in average BER expression, which is given by (22), are shown in Table III and if values higher than the upper limits are used, then the final average BER values will not change up to the sixth decimal place. Further, the upper limits used for truncating the infinite series of ergodic capacity bound in (30) are given in Table IV, and in the case of values greater than the upper limits, the final capacity values will remain unchanged until the sixth decimal place.

The convergence test of the derived average BER expression given by (22), which comprises an infinite series, is performed in Fig. 2(a). The average BER is plotted against the upper limit values of n for truncating the infinite series under different turbulence conditions and average SNR values. From the plots, it is clearly noticed that the value of average BER is constant for $n \geq 8$ under different average SNR values, which is also validated from Table III. Therefore, it can be inferred that the infinite series in the average BER expression convergences for $n \geq 8$. Similarly, the convergence test of the ergodic capacity expression given by (30) is performed in Fig. 2(b). The ergodic capacity bound is plotted against the upper limit values of n for truncating the infinite series under different average SNR values. The plots indicate that the ergodic capacity for $n \geq 10$

This article has been accepted for publication in IEEE Transactions on Communications. This is the author's version which has not been fully edited and content may change prior to final publication. Citation information: DOI 10.1109/TCOMM.2023.3278312

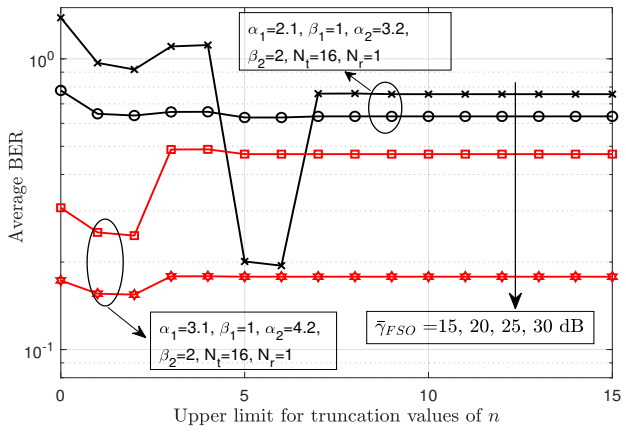

(a) Convergence test of the average BER given by (22)

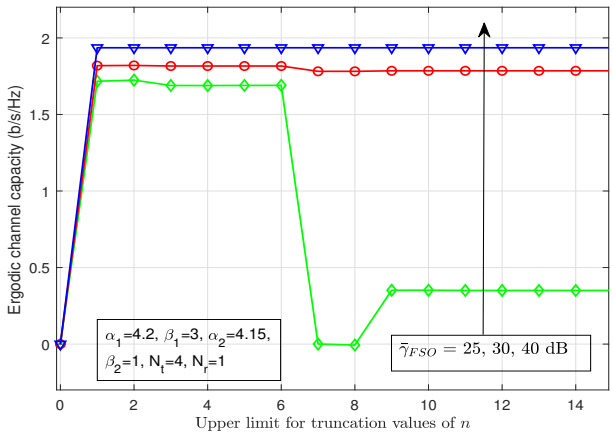

(b) Convergence test of the ergodic capacity given by (30)

Fig. 2: Convergence test for average BER and ergodic capacity expressions

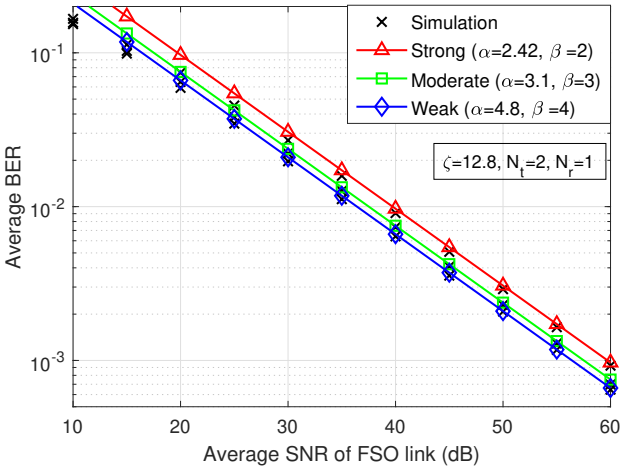

Fig. 3: Average BER under different turbulence conditions

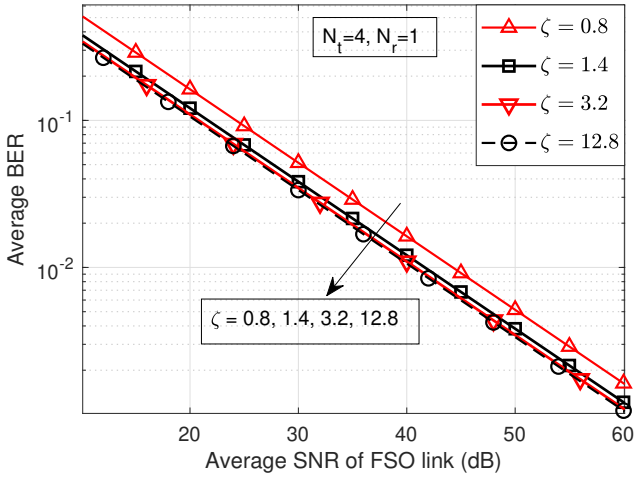

Fig. 4: Average BER for different pointing errors

remains constant under different average SNR values, which is also evident from Table IV.

Fig. 3 shows the average BER performance of the proposed system under different turbulence conditions. It can be seen from the plots that the performance improves with a decrease in turbulence severity. However, all the plots for different turbulence conditions have the same slope. This is because, the diversity gain of the OSSK-based MIMO-FSO system does not depend on the atmospheric turbulence conditions, which is also evident from (32). On the contrary, this inference is different as compared to the general PSK-based modulation techniques, where the diversity gain of the FSO-based system depends on the turbulence and pointing error parameters [15]–[16]. It is also to be noted that an SNR gain of around 4 dB is achieved to attain a BER of 10^{-2}, as the turbulence strength decreases from strong to weak. Further, the simulation plots almost coincide well with the theoretical upper bounds. This validates the correctness of our theoretical analysis.

In Fig. 4, the effect of pointing errors on the performance of the proposed system has been depicted. The turbulence parameters are assumed as $\alpha = 2.95$ and $\beta = 3$ for all pointing error conditions. From the plots, it is inferred that the performance is better for higher values of ζ. Because lower values of ζ imply higher pointing error severity, which deteriorates the system performance. The SNR gain of around 5 dB is achieved to attain the BER of 10^{-2} for high pointing errors scenario (i.e. $\zeta = 0.8$) over low pointing errors scenario (i.e. $\zeta = 12.8$). Here, it can also be seen that the slope is same for all plots and the diversity gain is independent of the channel parameters, as mentioned in Fig. 3. It also indicates that the effect of pointing errors is less on the OSSK-based FSO system.

In Fig. 5, we investigate the average BER performance of the proposed system model for different values of N_t and N_r by assuming $\alpha = 2.4$, $\beta = 2$, and $\zeta = 12.8$. It is observed in Fig. 5(a) that the performance of $N_t \times 1$ system degrades with increasing N_t. However, the spectral efficiency, which is given by $\log_2 N_t$ bits/s/Hz, increases with increasing N_t. Therefore, there is a trade-off between spectral efficiency and average BER in the case of an OSSK-based FSO system. This is because, the probability of error in detecting the index of the transmitting antenna increases as N_t increases. By substituting $\sum_{i=1}^{N_t}\sum_{j=1}^{N_t} d_H(s_j, s_i) = \frac{N_t^2 \log_2 N_t}{2}$ in (15) and assuming low SNR condition (i.e. $\bar{\gamma}_{FSO} \to 0$), the upper bound on BER after simplification can be written as BER $\leq N_t/4$. Since the BER is linearly varying with N_t, the average BER is not significantly tight, especially at low SNR values. However,

This article has been accepted for publication in IEEE Transactions on Communications. This is the author's version which has not been fully edited and content may change prior to final publication. Citation information: DOI 10.1109/TCOMM.2023.3278312

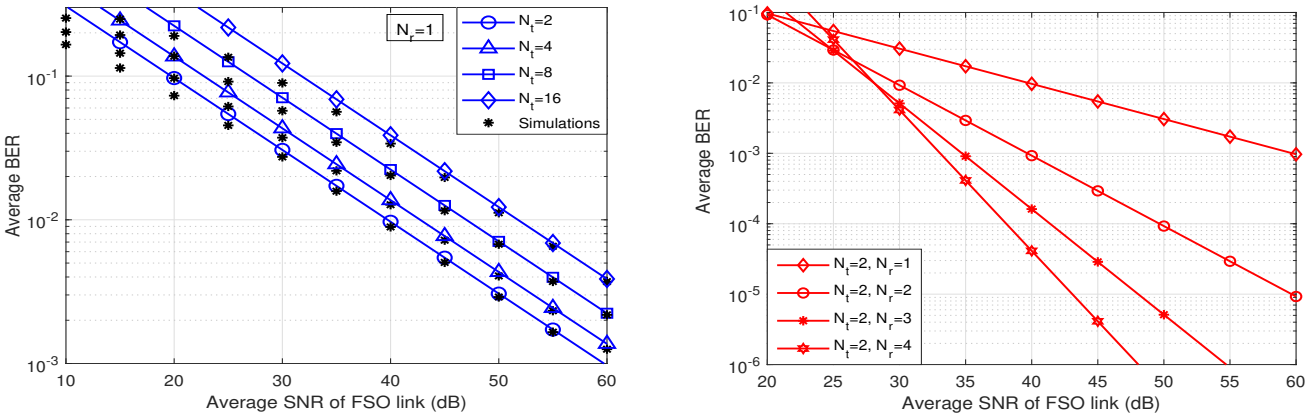

(a) (b)

Fig. 5: Average BER performance for different N_t and N_r

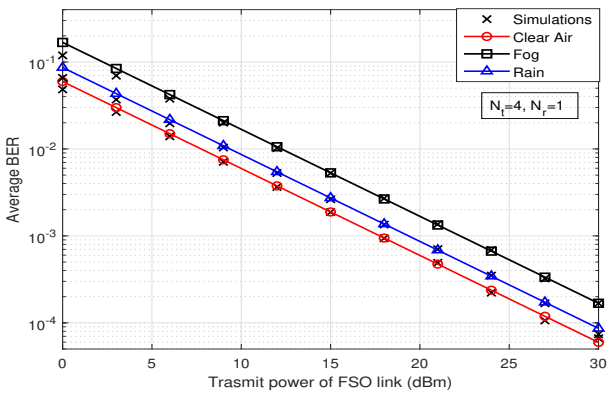

Fig. 6: Average BER performance for different weather conditions

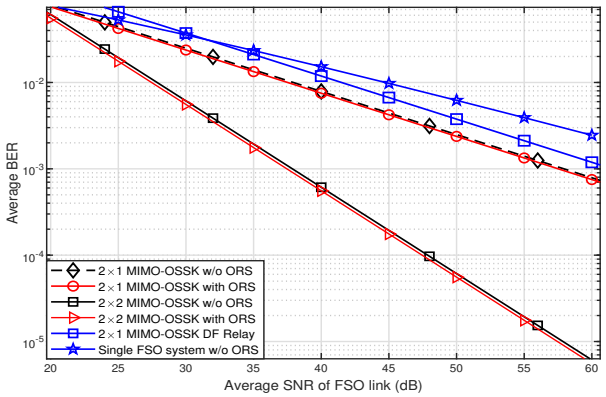

Fig. 7: Performance comparison of different FSO systems

the upper bound on average BER is tightly matching with the simulation results as the SNR increases, which is observed in Fig. 5(a) for $N_t = 8$ and 16.

In Fig. 5(b), the average BER is shown for different N_r assuming $N_t = 2$. It can be clearly seen that the average BER of the $N_t \times N_r$ system drastically improves with the increasing number of receiving apertures N_r, especially in the high-SNR regime. It is also evident from Fig. 5(b) that the diversity gain of the proposed system depends on the value of N_r, since the slope of the BER curves increases with an increase in N_r. Further, the SNR gain obtained by $N_r = 2$ over $N_r = 1$ is 20 dB to achieve a BER value of 10^{-3}. Similarly, the SNR gain achieved by $N_r = 3$ and $N_r = 4$ over $N_r = 2$ and $N_r = 3$ are 5 dB and 2 dB, respectively. Thus, it can be inferred that the SNR gain decreases with increasing N_r. Note that the diversity gain is calculated in Section III-C as $N_r/2$ and the same is also justified in Fig. 5(b).

In Fig. 6, the performance of the proposed system is given for different weather conditions by plotting the average BER against the transmit power. The values of the parameters are assumed as $\alpha = 2.62$, $\beta = 2$, and α_w (in dB/km) = 0.43, 20, and 5.8 for clear air, foggy, and rainy weather conditions, respectively. From the plots, it can be observed that the proposed system performs better in clear air compared to rainy and foggy weather conditions due to less atmospheric attenuation. Since the FSO system is more prone to foggy weather condition compared to rainy condition, the performance deteriorates more under foggy condition. It is clear from the plots that foggy condition requires 12 dBm of transmit power to attain an average BER value of 10^{-2}. However, clear air and rainy conditions require only 8 dBm and 9 dBm of transmit power values to attain the same BER, respectively.

Fig. 7 shows the performance comparison of the ORS-assisted OSSK-based MIMO-FSO system in terms of average BER with the following conventional FSO systems: (a) Single-link FSO system without ORS, (b) OSSK-based MIMO-FSO system without ORS and (c) OSSK-based dual-hop (DH) DF relaying system. The parameter values are assumed as $\alpha = 2.95$ and $\beta = 3$. It can be clearly seen that the proposed system achieves almost similar or slightly better performance than the OSSK system without ORS. As expected, the performance of a conventional single-link FSO system without ORS is the worst among all the FSO-based systems and the proposed ORS-assisted FSO system achieves an SNR gain of 7 dB at a BER of 10^{-2}. In addition, the OSSK-based DF relaying system performs better than the single-link FSO system. However, the OSSK-based DF relaying system performs inferior compared to the proposed system, with an SNR loss of 5 dB to attain the BER of 10^{-2}. This is mainly due to the fact that the impact of decoding errors in a relaying system is far more severe than the impact of cascaded channel turbulence in the ORS-based FSO system. It is also to be noted that the OSSK-based FSO system without ORS requires the presence of a direct LoS link for message transmission. Therefore, it is inferred that in the

This article has been accepted for publication in IEEE Transactions on Communications. This is the author's version which has not been fully edited and content may change prior to final publication. Citation information: DOI 10.1109/TCOMM.2023.3278312

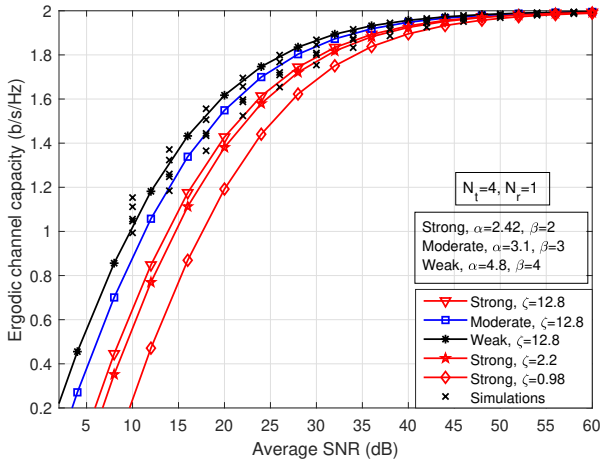

Fig. 8: Capacity performance for different turbulence and pointing errors conditions

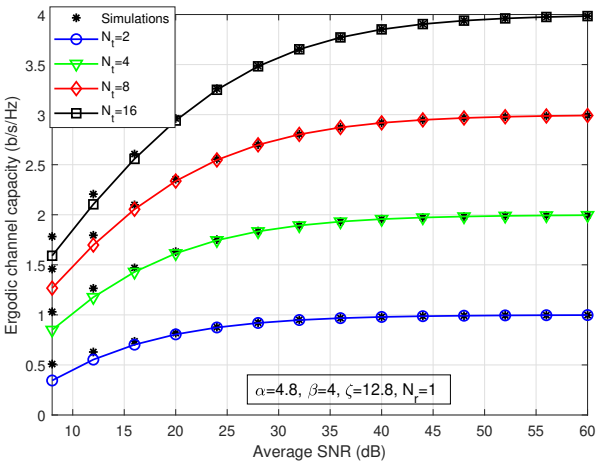

Fig. 9: Capacity performance for different N_t

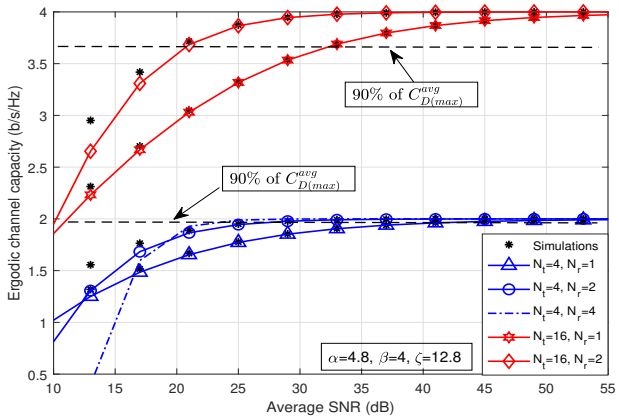

Fig. 10: Capacity performance for different N_r

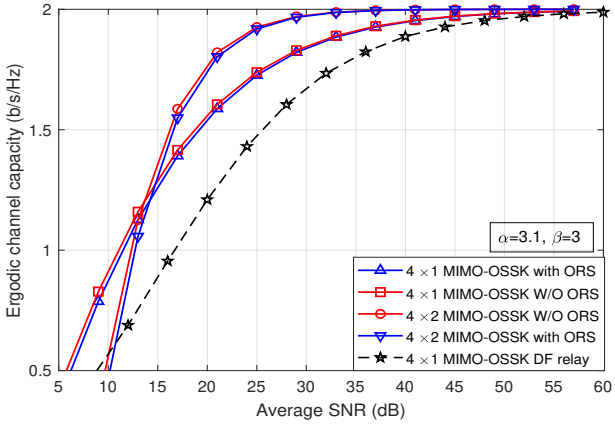

Fig. 11: Capacity performance comparison of various MIMO systems

absence of a direct link, the proposed ORS-assisted system can create a virtual direct LoS link with equal or slightly better BER performance than the existing OSSK-based MIMO system without ORS [27].

Fig. 8 shows the ergodic capacity performance under different turbulence and pointing error conditions. It can be observed that the performance of the proposed system declines as the turbulence severity increases. However, the difference in the performance after reaching 90% of the maximum achievable capacity $C^{avg}_{D(\max)}$ is very less. Similarly, as the pointing error severity increases (i.e. value of ζ decreases), the performance of the system degrades and there is around 5 dB SNR improvement from $\zeta = 0.98$ to $\zeta = 12.8$ under the strong turbulence condition to attain 90% of $C^{avg}_{D(\max)}$ value.

In Fig. 9, the ergodic capacity is given for different number of transmitting apertures $N_t = 2$, 4, 8, and 16. The plots show that the proposed system performs much better with an increase in N_t as expected. It is also confirmed from the plots that the maximum capacity for different N_t is obtained as $C^{avg}_{D(\max)} = \log_2 N_t$, which validates the derived expression for $C^{avg}_{D(\max)}$ in (26). Further, from Fig. 10, it is observed that there is a significant improvement in the capacity performance with an increase in N_r. It can also be noticed that there is a 7 dB SNR gain when $N_t = 4$ for $N_r = 2$ over $N_r = 1$ to achieve 90% of $C^{avg}_{D(\max)}$. Similarly, around 10 dB SNR gain is noticed by increasing N_r for the case when $N_t = 16$. From Fig. 10, it is clear that the SNR values required to achieve the maximum capacity is reduced by increasing N_r, as mentioned in Section III-C after (34). Furthermore, in Fig. 8, 9, and 10, Monte-Carlo simulations are closely matching with the theoretical lower bound results as evident from the figure, especially after the system achieves 90% of $C^{avg}_{D(\max)}$, which establishes the correctness of our derived lower bound expressions.

In Fig. 11, the proposed ORS-based OSSK system is compared with the OSSK-based MIMO-FSO system without ORS [27] and DF relaying-based OSSK system in terms of ergodic capacity. It can be clearly observed from the plots that the proposed ORS system achieves similar capacity performance equivalent to the OSSK system without ORS. However, as already mentioned, the ORS-assisted OSSK system does not require the presence of LoS link compared to the OSSK system without ORS. Thus, similar to BER performance in Fig. 7, it is inferred that a virtual LoS path is created using ORS without any significant degradation in the capacity performance. Further, the DF relaying-based system performs inferior compared to OSSK-based systems with ORS due to the fact that the impact of the worst channel among S to R (relay) and R to D links in a relaying system is far more severe than the effect of cascaded channel gain in the ORS-assisted system.

In summary, six significant technical findings or insights in this work are given as follows:

- For the proposed ORS-assisted OSSK-based FSO system, statistical functions of absolute difference between two cascaded FSO channels and instantaneous SNR are obtained. Further, from the statistical functions, closed-form expressions for two different performance metrics are derived for analysing the end-to-end system performance.
- The proposed ORS-assisted FSO system is highly beneficial, in case if a direct LoS path is not available between the source and the destination. This is because, it performs almost similar or slightly better than the FSO system without ORS, which alleviates the requirement of LoS path in FSO communication.
- Asymptotic analysis shows that the diversity gain of the proposed system is equal to $N_r/2$. Thus, the performance of the system improves with increasing number of receiving apertures N_r.
- Since the diversity gain does not depend on the channel parameters, high diversity gain shall be retained even under strong turbulence and high pointing error severity conditions.
- In addition, when turbulence fluctuates among weak, moderate, and strong turbulence conditions, the average BER of ORS-assisted OSSK-based MIMO-FSO is not changing significantly unlike conventional FSO systems.
- The proposed system performs better than a DF relaying-based OSSK system in terms of average BER and ergodic capacity without any additional signal processing or energy requirements. Hence, ORS-assisted FSO system can be proposed as an alternative to DF-relaying-based FSO system.

V. Conclusions

In this paper, we proposed an ORS-assisted OSSK-based MIMO-FSO system with an aim of mitigating the blockage in OSSK-based MIMO FSO systems. We derived the closed-form expressions for PDF of the absolute difference between two cascaded FSO channels, PDF of instantaneous SNR, and MGF of the instantaneous SNR. Further, with the help of the aforementioned expressions, the average PEP, the upper bound on average BER, and lower bound on ergodic capacity were evaluated over Malaga distributed turbulence along with pointing errors. Further, asymptotic expressions for average BER and ergodic capacity were derived and diversity gain of the proposed system was also obtained. The numerical results showed that the average BER and ergodic capacity performances were significantly improved as N_r increases and the maximum capacity achieved was $\log_2 N_t$. It was also confirmed from the analytical results that the effect of turbulence and pointing errors on the performance of the proposed system was not very significant, unlike the conventional FSO system, due to the usage of the OSSK scheme. Since ORS is assumed to be equivalent to a reflecting mirror which redirects the incident optical signal to the destination receiver with non-reconfigurable surfaces, the performance is almost similar or slightly better than the system without ORS. This alleviates the requirement of LoS transmission for the OSSK-based MIMO-FSO system and the proposed system also emerged as a better alternative to the DF relaying system.

Appendix A
Proof of Theorem 1

We assume $U_{kij} = |Z_{kij}|$, where $Z_{kij} = h_{ki} - h_{kj}$. Utilizing [27, eq. (9)], the PDF of Z_{kij} is given by

$$f_{Z_{kij}}(z) = \int_0^\infty f_{h_{ki}}(z+x) f_{h_{kj}}(x) dx. \tag{38}$$

Substituting $f_{h_{ki}}(\cdot)$ and $f_{h_{kj}}(\cdot)$ from (14) in (38) and employing [42, eq. (2.24.1.3)], we get the PDF of $f_{Z_{kij}}(z)$ as

$$f_{Z_{kij}}(z) = \frac{(A_1 A_2 \zeta)^2 B_1 B_2}{16 A_0 h_\ell} \sum_{p=1}^{\beta_1} \sum_{q=1}^{\beta_2} \sum_{r=1}^{\beta_1} \sum_{s=1}^{\beta_2} b_p^{(1)} b_q^{(2)} b_r^{(1)} b_s^{(2)} \times \sum_{n=0}^{\infty} \left(\frac{-B_1 B_2}{A_0 h_\ell} \right)^n \frac{z^n}{n!} G_{7\,7}^{5\,6} \left(1 \middle| \begin{matrix} \mathcal{N}_3 \\ \mathcal{N}_4 \end{matrix} \right), \tag{39}$$

where $\mathcal{N}_3 = [0, n-\zeta+1, n-\alpha_2+1, n-q+1, n-\alpha_1+1, n-p+1, \zeta]$ and $\mathcal{N}_4 = [\zeta-1, \alpha_2-1, s-1, \alpha_1-1, r-1, n-\zeta, n]$. Therefore, the PDF of U_{kij} can be written as [27]

$$f_{U_{kij}}(u) = 2 f_{Z_{kij}}(u). \tag{40}$$

Further, by substituting (39) in (40), the final expression for $f_{U_{kij}}(u)$ is obtained as (17).

Appendix B
Proof of Theorem 2

The PDF of the instantaneous SNR of k^{th} FSO link $\gamma_{kij} = U_{kij}^2 \overline{\gamma}_{FSO}$ is written in terms of PDF of Z_{kij} as

$$f_{\gamma_{kij}}(\gamma) = \frac{1}{\sqrt{\gamma \overline{\gamma}_{FSO}}} f_{Z_{kij}} \left(\sqrt{\frac{\gamma}{\overline{\gamma}_{FSO}}} \right). \tag{41}$$

Substituting $f_{Z_{kij}}(\cdot)$ from (39) in (41), we get the PDF of γ_{kij} as

$$f_{\gamma_{kij}}(\gamma) = \frac{(A_1 A_2 \zeta)^2 B_1 B_2}{16 A_0 h_\ell} \sum_{p=1}^{\beta_1} \sum_{q=1}^{\beta_2} \sum_{r=1}^{\beta_1} \sum_{s=1}^{\beta_2} b_p^{(1)} b_q^{(2)} b_r^{(1)} b_s^{(2)} \times \sum_{n=0}^{\infty} \left(\frac{-B_1 B_2}{A_0 h_\ell} \right)^n \frac{\gamma^{\frac{n-1}{2}}}{n! \overline{\gamma}_{FSO}^{\frac{n+1}{2}}} G_{7\,7}^{5\,6} \left(1 \middle| \begin{matrix} \mathcal{N}_3 \\ \mathcal{N}_4 \end{matrix} \right) \tag{42}$$

Further, to calculate the PDF of overall instantaneous SNR, which is given as $\gamma_{ij} = \overline{\gamma}_{FSO} \sum_{k=1}^{N_r} U_{kij}^2 = \sum_{k=1}^{N_r} \gamma_{kij}$, we use MGF-based approach. The MGF of the γ_{ij} is given by

$$\Psi_{\gamma_{ij}}(-t) = \prod_{k=1}^{N_r} \Psi_{\gamma_{kij}}(-t), \tag{43}$$

where $\Psi_{\gamma_{kij}}(-t)$ is the MGF of γ_{kij} and is calculated as

$$\Psi_{\gamma_{kij}}(-t) = \sum_{n=0}^{\infty} C_n t^{-\frac{n+1}{2}}, \tag{44}$$

where

$$C_n = \frac{(A_1 A_2 \zeta)^2 B_1 B_2}{16 A_0 h_\ell} \sum_{p=1}^{\beta_1} \sum_{q=1}^{\beta_2} \sum_{r=1}^{\beta_1} \sum_{s=1}^{\beta_2} b_p^{(1)} b_q^{(2)} b_r^{(1)} b_s^{(2)} \times \left(\frac{-B_1 B_2}{A_0 h_\ell} \right)^n \frac{\Gamma\left(\frac{n+1}{2}\right)}{n! \overline{\gamma}_{FSO}^{\frac{n+1}{2}}} G_{7\,7}^{5\,6} \left(1 \middle| \begin{matrix} \mathcal{N}_3 \\ \mathcal{N}_4 \end{matrix} \right) \tag{45}$$

Substituting (44) in (43) and utilizing [41, eq. (0.314)], we can write $\Psi_{\gamma_{ij}}(-t)$ as

$$\Psi_{\gamma_{ij}}(-t) = \sum_{n=0}^{\infty} D_n t^{-\frac{n+N_r}{2}}, \tag{46}$$

where $D_0 = C_0^{N_r}$ and $D_u = \frac{1}{uC_0} \sum_{m=1}^{u} (mN_r - u + m) C_m D_{u-m}$. Further, by taking the inverse Laplace transform of $\Psi_{\gamma_{ij}}(-t)$, the PDF of γ_{ij} can be obtained as (18).

REFERENCES

[1] M. Z. Chowdhury, M. Shahjalal, S. Ahmed, and Y. M. Jang, "6G wireless communication systems: Applications, requirements, technologies, challenges, and research directions," *IEEE Open J. Commun. Soc.*, vol. 1, pp. 957-975, 2020.

[2] Q. Wu, S. Zhang, B. Zheng, C. You, and R. Zhang, "Intelligent reflecting surface-aided wireless communications: A tutorial," *IEEE Trans. Commun.*, vol. 69, no. 5, pp. 3313-3351, May 2021.

[3] E. Basar and I. Yildirim, "Reconfigurable intelligent surfaces for future wireless networks: A channel modeling perspective," *IEEE Wireless Commun.*, vol. 28, no. 3, pp. 108-114, June 2021.

[4] J. Xu, C. Yuen, C. Huang, N. U. Hassan, G. C. Alexandropoulos, M. D. Renzo, and M. Debbah, "Reconfiguring wireless environments via intelligent surfaces for 6G: reflection, modulation, and security," *Science China Information Sciences*, vol. 66, Issue 3, 2023.

[5] E. Basar, M. Di Renzo, J. De Rosny, M. Debbah, M. -S. Alouini, and R. Zhang, "Wireless communications through reconfigurable intelligent surfaces," *IEEE Access*, vol. 7, pp. 116753-116773, 2019.

[6] A. M. Salhab and M. H. Samuh, "Accurate Performance Analysis of Reconfigurable Intelligent Surfaces Over Rician Fading Channels," *IEEE Wireless Commun. Lett.*, vol. 10, no. 5, pp. 1051-1055, May 2021.

[7] D. Tyrovolas, S. A. Tegos, E. C. Dimitriadou-Panidou, P. D. Diamantoulakis, C. K. Liaskos, and G. K. Karagiannidis, "Performance analysis of cascaded reconfigurable intelligent surface networks," *IEEE Wireless Commun. Lett.*, vol. 11, no. 9, pp. 1855-1859, Sept. 2022.

[8] J. Yao, J. Xu, W. Xu, C. Yuen, and X. You, "A Universal Framework of Superimposed RIS-Phase Modulation for MISO Communication," *IEEE Trans. Veh. Technol.*, early access, Nov. 2022.

[9] M. Z. Chowdhury, M. K. Hasan, M. Shahjalal, M. T. Hossan, and Y. M. Jang, "Optical wireless hybrid networks: Trends, opportunities, challenges, and research directions," *IEEE Commun. Surveys Tut.*, vol. 22, no. 2, pp. 930-966, Secondquarter 2020.

[10] S. A. Al-Gailani et al., "A survey of free space optics (FSO) communication systems, links, and networks," *IEEE Access*, vol. 9, pp. 7353-7373, 2021.

[11] H. Kazemi and M. Uysal, "Performance analysis of MIMO free-space optical communication systems with selection combining," *in proc. 21st Signal Processing and Communications Applications Conference (SIU)*, 2013, pp. 1-4.

[12] S. Malik and P. K. Sahu, "M-ary phase-shift keying-based single-input-multiple-output free space optical communication system with pointing errors over a gamma–gamma fading channel," *Appl. Opt.*, vol. 59, pp. 59-67, Dec. 2020.

[13] M. R. Bhatnagar, "Performance analysis of decode-and-forward relaying in Gamma-Gamma fading channels," *IEEE Photon. Technol. Lett.*, vol. 24, no. 7, pp. 545-547, 2012.

[14] E. Zedini and M. -S. Alouini, "On the performance of multihop heterodyne FSO systems with pointing errors," *IEEE Photon. J.*, vol. 7, no. 2, pp. 1-10, April 2015.

[15] M. R. Bhatnagar and Z. Ghassemlooy, "Performance analysis of Gamma–Gamma fading FSO MIMO links with pointing errors," *J. Lightw. Technol.*, vol. 34, no. 9, pp. 2158-2169, May 2016.

[16] N. Vishwakarma and Swaminathan R, "On the maximal-ratio combining of FSO and RF links over generalized distributions and its applications in hybrid FSO/RF systems," *Opt. Commun.*, vol. 520, Oct. 2022.

[17] O. S. Badarneh and R. Mesleh, "Diversity analysis of simultaneous mmWave and free-space-optical transmission over $\mathcal{F}$-distribution channel models," J. Opt. Commun. Netw., vol. 12, no. 11, pp. 324-334, Nov. 2020.

[18] S. Sharma, A. Madhukumar, and Swaminathan R, "MIMO hybrid FSO/RF system over generalized fading channels," *IEEE Trans. Veh. Technol.*, vol. 70, no. 11, pp. 11565-11581, Nov. 2021.

[19] B. Bag, A. Das, C. Bose, and A. Chandra, "Improving the performance of a DF relay-aided FSO system with an additional source–relay mmWave RF backup," J. Opt. Commun. Netw., vol. 12, no. 12, pp. 390-402, Dec. 2020.

[20] R. Mesleh, H. Elgala, and H. Haas, "Optical spatial modulation," *J. Opt. Commun. Netw.*, vol. 3, no. 3, pp. 234–244, Mar. 2011.

[21] S. Yu, C. Geng, J. Zhong, and D. Kang, "Performance analysis of optical spatial modulation over a correlated Gamma–Gamma turbulence channel," *Appl. Opt.*, vol. 61, pp. 2025-2035, 2022.

[22] T. Fath and H. Haas, "Optical spatial modulation using colour LEDs," *in proc. 2013 IEEE Int. Conf. Commun. (ICC)*, Budapest, Hungary, 2013, pp. 3938-3942.

[23] M. Abazaa, R. Mesleha, A. Mansourb, and M. Aggoune, "The performance of space shift keying for free-space optical communications over turbulent channels," *Proc. SPIE*, vol. 9387, 93870V, 2015.

[24] A. Jaiswal, M. R. Bhatnagar, and V. K. Jain, "Performance evaluation of space shift keying in free-space optical communication," *J. Opt. Commun. Netw.*, vol. 9, no. 2, pp. 149-160, Feb. 2017.

[25] I. Chauhan, P. Paul, M. R. Bhatnagar, and J. Nebhen, "Performance of optical space shift keying under jamming," *Appl. Opt.*, vol. 60, pp. 1856-1863, 2021.

[26] A. Jaiswal, M. R. Bhatnagar, and V. K. Jain, "On the ergodic capacity of optical space shift keying based FSO-MIMO system under atmospheric turbulence," *in Proc. IEEE ICC*, 2017, pp. 1-7.

[27] A. Jaiswal, M. Abaza, M. R. Bhatnagar, and V. K. Jain, "An investigation of performance and diversity property of optical space shift keying-based FSO-MIMO system," *IEEE Trans. Commun.*, vol. 66, no. 9, pp. 4028-4042, Sept. 2018.

[28] H. Wang, Z. Zhang, B. Zhu, J. Dang, L. Wu, L. Wang, K. Zhang, and Y. Zhang, "Performance of wireless optical communication with reconfigurable intelligent surfaces and random obstacles," [Online]. Available: https://arxiv.org/abs/2001.057157.

[29] M. Najafi, B. Schmauss, and R. Schober, "Intelligent reflecting surfaces for free space optical communication systems," *IEEE Trans. Commun.*, vol. 69, no. 9, pp. 6134-6151, Sept. 2021.

[30] M. Di Renzo et al., "Reconfigurable intelligent surfaces vs. relaying: differences, similarities, and performance comparison," *IEEE Open J. Commun. Soc.*, vol. 1, pp. 798-807, 2020.

[31] A. R. Ndjiongue, T. M. N. Ngatched, O. A. Dobre, A. G. Armada, and H. Haas, "Analysis of RIS-based terrestrial-FSO link over G-G turbulence with distance and jitter ratios," *J. Lightw. Technol.*, vol. 39, no. 21, pp. 6746-6758, Nov. 2021.

[32] L. Yang, W. Guo, D. B. Costa, and M.-S. Alouini, "Free-space optical communication with reconfigurable intelligent surfaces," [Online]. Available: https://doi.org/10.48550/arXiv.2012.0054

[33] V. K. Chapala and S. M. Zafaruddin, "Unified performance analysis of reconfigurable intelligent surface empowered free-space optical communications," *IEEE Trans. Commun.*, vol. 70, no. 4, pp. 2575-2592, April 2022.

[34] A. M. Salhab and L. Yang, "Mixed RF/FSO Relay Networks: RIS-Equipped RF Source vs RIS-Aided RF Source," *IEEE Wireless Commun. Lett.*, vol. 10, no. 8, pp. 1712-1716, Aug. 2021.

[35] S. Sharma, N. Vishwakarma, and Swaminathan R., "Performance Analysis of IRS-Assisted Hybrid FSO/RF Communication System," *in proc. 2022 National Conference on Communications (NCC)*, 2022, pp. 268-273.

[36] S. Malik, P. Saxena, and Y. H. Chung, "Performance analysis of a UAV-based IRS-assisted hybrid RF/FSO link with pointing and phase shift errors," *J. Opt. Commun. Netw.*, vol. 14, no. 4, pp. 303-315, April 2022.

[37] I. S. Ansari, F. Yilmaz, and M. Alouini, "Performance analysis of free-space optical links over Málaga ($\mathcal{M}$) turbulence channels with pointing errors," *IEEE Trans. Wireless Commun.*, vol. 15, no. 1, pp. 91-102, Jan. 2016.

[38] A. J. Navas, J. M. G. Balsells, J. F. Paris, and A. P. Notario, " A unifying statistical model for atmospheric optical scintillation," *Numerical Simulations of Physical and Engineering Processes*, J. Awrejcewicz, Ed. Intech, 2011, ch. 8.

[39] Wolfram Research Inc., *Mathematica Edition: Version 8*, Champaign, IL, USA, 2010. [Online]. Available: https://functions.wolfram.com/HypergeometricFunctions/MeijerG/

[40] W. N. Edward and M. Geller, "A table of integrals of the error functions,"*J. Res. Nat. Bur. Stand.*, vol. 73B, no. 1, pp. 1–20, Oct. 1968.

[41] I. S. Gradshteyn and I. M. Ryzhik, *Table of Integrals, Series, and Products*, 7th ed. Academic, 2007.

[42] A. P. Prudnikov, Y. A. Brychkov, and O. I. Marichev, *Integrals and Series. Gordon and Breach*, vol. 3, 1990.

This article has been accepted for publication in IEEE Transactions on Communications. This is the author's version which has not been fully edited and content may change prior to final publication. Citation information: DOI 10.1109/TCOMM.2023.3278312

Narendra Vishwakarma (Student Member, IEEE) received the B.E. degree in electronics and communication engineering from RGPV, Bhopal, India, and the M.Tech. degree in computer technology from IIT Delhi, India. He is currently pursuing the Ph.D. degree in the Department of Electrical Engineering, IIT Indore under Prime Minister's Research Fellows (PMRF) scholarship. His current research interests include the design and analysis of hybrid free space optics/radio frequency communication systems, performance analysis of wireless digital communication systems over generalized fading models, intelligent-reflecting-surfaces (IRS)-aided wireless communications, next-generation terrestrial communication, and satellite communication systems.

Dr. Swaminathan R (Senior Member, IEEE) received the B.Tech. degree in electronics and communication engineering from SASTRA University, Thanjavur, in 2009, the M.E. degree in communication systems from the College of Engineering Guindy, Anna University, Chennai, in 2011, and the Ph.D. degree from IIT Kharagpur, in 2016. He worked as a Postdoctoral Research Fellow with Nanyang Technological University (NTU), Singapore, from 2015 to 2019. He is currently working as an Assistant Professor with the Department of Electrical Engineering, IIT Indore. He is also associated with Center of Futuristic Defense and Space Technology (CFDST), Center for Electric Vehicle and Intelligent Transport Systems (CEVITS) at IIT Indore. He is currently serving as a CEO of IITI Advanced Centre for Entrepreneurship (ACE) Foundation (i.e. Incubation Centre of IIT Indore) and also as a Professor-In-Charge of Centre for Entrepreneurship Education and Development (CEED), IIT Indore. He is the author or co-author of more than 60 reputed journal and IEEE conference publications. His current research interests include broad areas in Wireless Communications, Communication Systems and Coding Theory. He received the Gold Medal from the College of Engineering Guindy, Anna University. He has given invited talks on entrepreneurship and wireless communications on several occasions at leading engineering institutions. He has organized four faculty development programs (FDPs), short-term courses (STCs), and workshops funded by SERB, ATAL Academy, AICTE-QIP, and TEQIP-III. Further, he has also secured three funded research projects from DST-SERB worth of more than Rs 50 Lakhs and successfully completed two consultancy projects for Airtel and Danish Management, Denmark (consulting firm for India-European Union standardization project). He has been serving as a reviewer for reputed IEEE journals and as a TPC member for reputed IEEE conferences. He has been honoured as an Exemplary Reviewer by IEEE Communications Society, USA for the year 2021 towards significant contributions in reviewing IEEE Communications Letters journal.

Panagiotis D. Diamantoulakis (Senior Member, IEEE) received the Diploma (five years) and the Ph.D. degree from the Department of Electrical and Computer Engineering, Aristotle University of Thessaloniki, Thessaloniki, Greece, in 2012 and 2017, respectively. Since 2017, he has been a Postdoctoral Fellow with Wireless Communications and Information Processing (WCIP) Group, AUTH and since 2021, he has been a Visiting Assistant Professor with the Key Lab of Information Coding and Transmission, Southwest Jiaotong University, Chengdu, China. Since 2022 he has also been a Postdoctoral Fellow with the Department of Applied Informatics, University of Macedonia, Thessaloniki, Greece. His research interests include optimization theory and applications in wireless networks and smart grids, game theory, goal-oriented communications, and optical wireless communications. He is also an Editor of IEEE Open Journal of the Communications Society, Physical Communications (Elsevier), and Frontiers in Communications and Networks, while during 2018-2023 he was an Editor of IEEE Wireless Communications Letters.

George K. Karagiannidis ((M'96-SM'03-F'14) is currently Professor in the Electrical & Computer Engineering Dept. of Aristotle University of Thessaloniki, Greece and Head of Wireless Communications & Information Processing (WCIP) Group. He is also Faculty Fellow in the Cyber Security Systems and Applied AI Research Center, Lebanese American University. His research interests are in the areas of Wireless Communications Systems and Networks, Signal processing, Optical Wireless Communications, Wireless Power Transfer and Applications and Communications & Signal Processing for Biomedical Engineering. Dr. Karagiannidis was in the past Editor in several IEEE journals and from 2012 to 2015 he was the Editor-in Chief of IEEE Communications Letters. From September 2018 to June 2022 he served as Associate Editor-in Chief of IEEE Open Journal of Communications Society. Currently, he is in the Steering Committee of IEEE Transactions on Cognitive Communications & Networks.

Recently, he received three prestigious awards: The 2021 IEEE ComSoc RCC Technical Recognition Award, the 2018 IEEE ComSoc SPCE Technical Recognition Award and the 2022 Humboldt Research Award from Alexander von Humboldt Foundation.

Dr. Karagiannidis is one of the highly-cited authors across all areas of Electrical Engineering, recognized from Clarivate Analytics as Web-of-Science Highly-Cited Researcher in the eight consecutive years 2015-2022.